Conference Proceedings

Solar World Congress 2015
Daegu, Korea, 08 – 12 November 2015

WIND PRESSURE DISTRIBUTION ON THROUGH CONCENTRATOR

Qiong Zou[1], Zhengnong Li[1], Honghua Wu[1], RaoKuang[2], Yi Hui[1]

[1] College of Civil Engineering, Hunan University, Changsha, Hunan Province, China

[2] Laboratory of Energy Thermal Conversion and Control of Ministry of Education, School of Energy and Environment, Southeast University, Nanjing, China

Abstract

Aiming to get a precise understanding of wind pressure distribution on trough concentrator surface, wind tunnel experiments on trough concentrator model were carried out in HD-3 atmospheric boundary layer wind tunnel at Hunan University in this study. The length scale of the trough concentrator was 1:15, and 324 measuring taps were arranged symmetrically on both sides, with 162 taps on each. The distribution contours of mean wind pressure coefficient and fluctuating wind pressure coefficients on mirror surface under typical working conditions were obtained. The variation of mean wind pressure coefficient of some taps with yaw angles and pitch angles were provided. Extreme wind pressure was calculated by Hermite moment-based method, and the extreme wind distribution was also presented in this article.

Keywords: *Trough Concentrator, Wind Tunnel Experiments, Wind Pressure Distribution, Hermite moment-based method,*

1. Introduction

From the beginning of the 70's of the last century, a lot of various experimental solar thermal power stations were invested in developed countries. Solar thermal power is a widely discussed research topic in engineering field, and trough solar power generation (shown in Fig.1) is an internationally dominating technique with a good commercialization prospect. Since solar thermal power stations are usually located in the open, flat areas, wind load has to be properly estimated. By studying wind pressure distribution on mirror surface of heliostat and parabolic dish collectors through boundary layer wind tunnel experiment, Peterka and Derickson put forward the algorithm of wind load design on heliostat and parabolic dish collectors. Hosoya and Peterka have conducted a series of wind tunnel tests. Their tests presented the peak load and the distribution of local pressure across the face of the solar collector.The research of wind load on heliostat surface with different Reynolds numbers was done by Pfahl. Naeenia and Yaghoubi studied trough solar concentrator by conducting numerical simulation and wind tunnel experiments, and different wind loads on mirror surface with different pitch angles. Gong introduced an algorithm for wind-induced response calculation. He also studied the wind load characteristics on mirror surface as well as the characteristics of wind field around a trough concentrator through on-site measurement.

doi:10.18086/swc.2015.10.05 Available at http://proceedings.ises.org

Fig. 1: Trough concentrator (The picture is from National solar thermal Union)

The trough concentrator surface is in an arch shape, thus it can be known that the wind pressure distribution on it is complex. However, there are quite a few researches have been done for the wind pressure distribution on such structures in China. And the wind resistance design of trough concentrator in China is thus in accordance with the existing specifications or technical standard of other countries. However, due to different geographical features and climate condition, the requirements on the strength and rigidity of the concentrator group cannot be met while designed in accordance with such codes. Although there have been some advances for trough collectors in wind tunnel testing and in field measurement, there are still some limiting aspects of the measurement. Compared with previous wind tunnel test, in this paper, in order to obtain more accurate experimental data, the number of wind pressure measuring taps has been increased to 324. In addition, this paper presented the distribution of mean and fluctuating wind pressure on mirror surface. Aiming to get a precise understanding of wind load distribution on trough concentrator surface, wind tunnel experiments on trough concentrator model were carried out in HD-3 atmospheric boundary layer wind tunnel at Hunan University in this study.

2. General information of the experiment

2.1. Experimental apparatus

The experiment was carried out in HD-3 atmospheric boundary layer wind tunnel in Wind Tunnel Laboratory of Hunan University. The wind tunnel was a straight type boundary-layer wind tunnel with low speed. The cross section of the experiment area had a width of 3 meters and a height of 2.5 meters, while the wind speed in the experimental segment was continuously tunable in the range of 0.5~20m·s-1. Cobra probe system could be applied to measure the mean wind speed, turbulence intensity and fluctuating wind power spectrum of flow fields. The pressure measuring apparatus was a DTCnet System made by PSI Corporation. The DTCnet System has 8 modules, and each module has 64 channels, the measuring range is 0.36PSI, with accuracy± 0.05%.

2.2. Experimental model

The trough concentrator prototype consisted of mirror surface, a supporting girder, left and right fin plates, a heat collecting pipe bracket, a transmission system and pillars on both sides. The horizontal projection of mirror surface was 12.2×6.75m, as shown in Fig.2. The mirror surface consisted of 96 small mirrors with a gap of 0.02~0.05m between them. The length scale of the trough concentrator was 1:15 (Fig.3). In order to measure the wind pressure on front and back mirror surface simultaneously in the pressure measuring experiment on mirror surface, 324 measuring taps were arranged symmetrically on both sides, with 162 taps on each. The measuring taps on front surface were arranged in a sequence from A~T, while the measuring taps on back side were arranged in the sequence of AX~TX corresponding to the taps on front surface, as shown in Fig.4. Since the length scale was small, the gaps between small mirrors in the prototype were ignored in experimental the model, the mirror surface in the experimental modal only consisted of two parts.

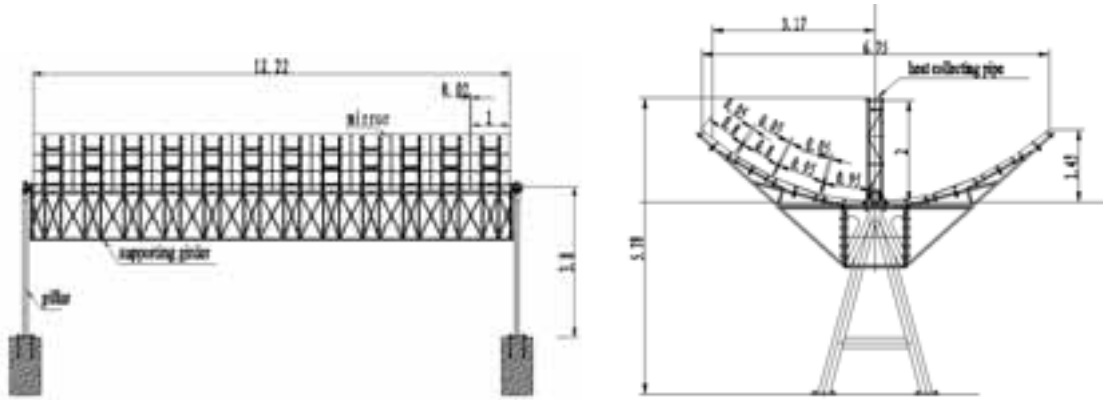

Fig.2: Structure of a trough concentrator

Fig.3: Model of a trough concentrator (1:15)

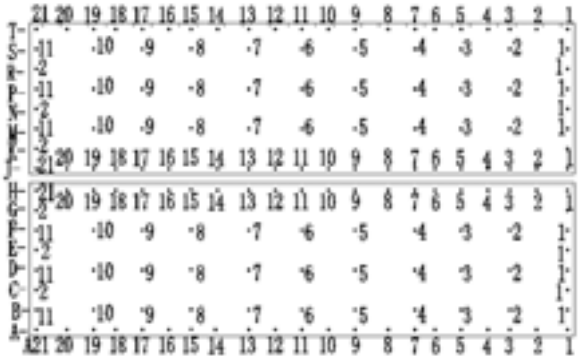

Fig.4: Layout of pressure measuring taps

2.3. Experimental conditions

In the wind tunnel experiment, the horizontal angle of concentrator θ increases from 0° to 180° in increments of 5 clockwise. The vertical elevation angle β of mirror surface increases from 0° to 90° in increments of 10 clock wise, totally 10 different angles. Consequently, 37*10=370 operating conditions are included. The sketch map of the angle of mirror is shown in Fig.5. Because the trough concentrator is a symmetric structure along X axis and Y axis, when the pitch angle is greater than 90°, for example, the pitch angle is 150°, and the yaw angle is 0°(150-000), the wind load of the trough solar collector of 150-000 condition is analogous to that of 30-180 condition. Therefore, we only measured the wind loads for the pitch angle in the range of 0°~90° in wind tunnel test. (Operating condition is expressed in the form of "pitch angle of mirror surface -yaw angle", for instance, 30-000 indicates an operating condition with pitch angle of 30 ^{o} and yaw angle of 0 ^{o}).

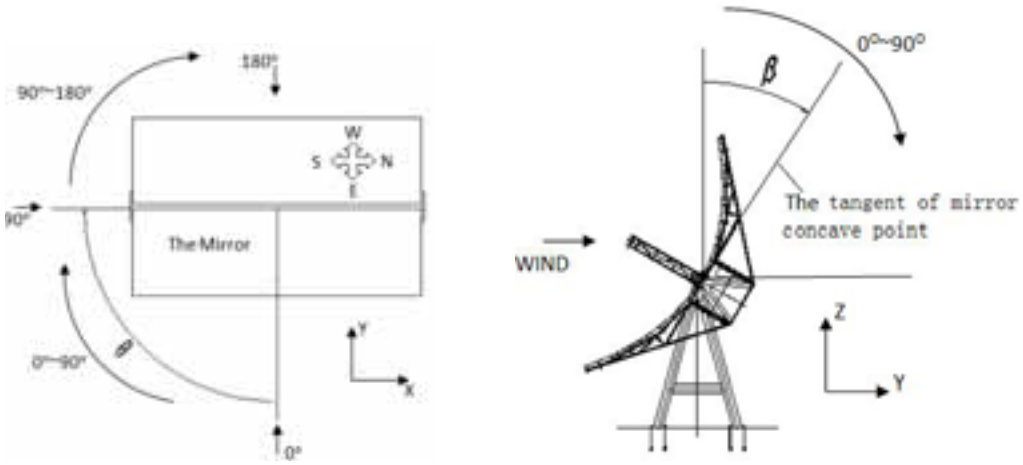

Fig.5: Horizontal wind angle of concentrator in wind tunnel

2.4. Wind field simulation

The comprehensive comparison for the near-ground wind field of wind load codes between China and Europe and America were made, including the mean velocity profile and turbulence intensity profile, fluctuating wind spectrum, etc. The mean velocity profiles of Chinese and Euro codes have a faster increase than other countries, but the mean velocity profile has little difference in the codes of different countries. Compared with other countries, the turbulence intensities in Chinese code are relatively small. For example, with terrain category B (such as the building sparse open country, suburb, forests) and at the height of 10m, the turbulence intensity value of Chinese code is 0.12, the minimum value of the other countries is 0.19, and the maximum value is 0.26.

Based on the terrain roughness characteristics of the site where the trough concentrator is located, the spire-roughness technique was used to simulate the atmospheric boundary layer wind field in wind tunnel according to international experiment method and current Chinese Code on terrain category B. Wind velocity profile is expressed by Equation (1):

$$V_z = V_b\left(\frac{Z}{Z_b}\right)^{\alpha} \qquad \text{(eq. 1)}$$

Where Z_b is the standard reference height; V_b is the mean wind speed at the standard reference height; Z is the height above ground; V_z is the wind speed at the height Z; α is the surface roughness index. The experiment in this study is to simulated terrain category B, so the value α was set to be 0.15 accordingly.

The turbulence intensity profile is calculated according to Equation (2) and (3):

$$I_z(z) = I_{10}\bar{I}_z(z) \qquad \text{(eq. 2)}$$

$$\bar{I}_z(z) = \left(\frac{Z}{10}\right)^{-d} \qquad \text{(eq. 3)}$$

where the turbulence intensity at the height of Z is $I_z(z)$; I_{10} is the nominal turbulence intensity at the height of 10m; the surface roughness index is set as 0.14 ; Z is the height above ground; d is 0.15. The wind velocity profile and turbulence intensity profile are shown in Fig. 6. The power spectrum of longitudinal fluctuating wind speed is compared with power spectrum by ESDU in Fig. 7.

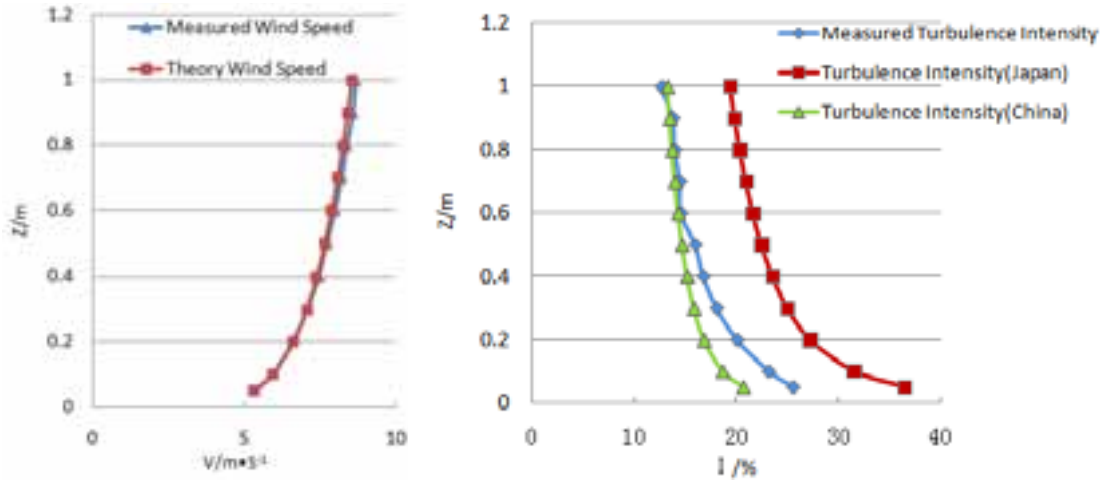

Fig. 6: Mean wind speed profile and the turbulence intensity profile

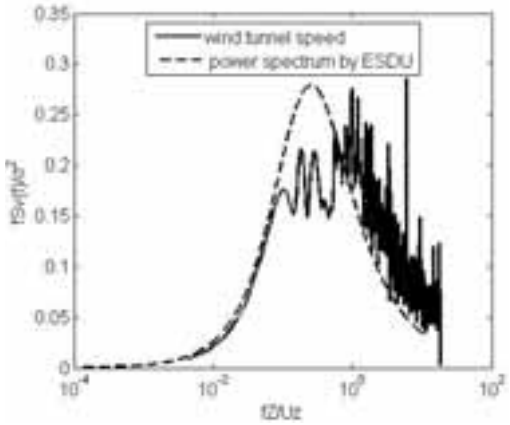

Fig. 7: Wind speed power spectrum of along wind fluctuating wind

3. Processing of experiment data

The measuring taps were arranged symmetrically at the same location on the front side and back side of mirror surface in wind tunnel experiment, respectively. Equation (4) is the calculation equation of net wind pressure coefficient for each measuring position on mirror surface:

$$C_{Pi}(t)=\frac{P_i^f(t)-P_i^b(t)}{\frac{1}{2}\rho V_H{}^2} \qquad \text{(eq. 4)}$$

where $C_{Pi}(t)$ is wind pressure coefficient; i is the serial number of measuring tap; $P_i^f(t)$ and $P_i^b(t)$ are the wind pressures of measuring taps on front side and backside (the leeward side when pitch angle and yaw angle are 0^o). With a sampling frequency of 312.5 Hz, 10000 P_i data were recorded for each measuring taps. ρ is the air density in experiment; V_H is the wind speed of the reference tap, and the height of the reference velocity is 0.67m which corresponds to a prototype height of 10m, which is in accordance with Chinese code[10]. By analyzing $C_{Pi}(t)$, the mean wind pressure coefficient, fluctuating wind pressure coefficient could be calculated according to Equation (5) ~(6).

$$C_{Pi,mean}=\frac{1}{N}\sum_{i=1}^{N}C_{Pi}(t) \qquad \text{(eq. 5)}$$

$$C_{Pi,rms}=\sqrt{\frac{1}{N-1}\sum_{i=1}^{N}\left(C_{Pi}(t)-C_{Pi,mean}\right)^{2}} \qquad \text{(eq. 6)}$$

where $C_{Pi,mean}$ is the mean wind pressure coefficient of the measuring tap i; $C_{Pi,rms}$ is the fluctuating wind pressure coefficient of the measuring tap i; $C_{pi}(t)$ is the time history value of the wind pressure coefficient of a certain measuring tap; i =1, 2, ..., N , N is the number of samples.

4. Distribution of wind pressure

4.1. Distribution of mean wind pressure

The contour map of mean wind pressure coefficient on mirror surface in typical operating condition is shown in Fig. 8.

As shown in Fig. 8, when yaw angle and pitch angle are 0°, the wind pressure coefficients on mirror surface are all positive values. The maximum value is located in the region a little above the middle part of mirror surface. As pitch angle increases, the position of the maximum wind pressure moves toward the edge of mirror surface in the windward. The maximum wind pressure appears at the edge as well as near the concave tap of the mirror surface because of its arch shape when pitch angle reaches 60°. This is different from the wind pressure distribution on heliostat surface. Wind pressure coefficient on the lower part of mirror surface becomes negative when pitch angle reaches 90°. When yaw angle increases to 45°, wind pressure coefficient starts to decrease from the edge of mirror in the windward to the leeward along with the increase of pitch angle. When yaw angle is 90°, pitch angle variation has little influence on wind pressure coefficient distribution because wind direction is parallel with mirror surface. Furthermore, the wind pressure coefficient on the whole mirror surface is small, varying from 0.04 to 0.67. When yaw angle is 135°, wind pressure coefficients on mirror surface are generally negative because the back side of mirror surface is windward, and maximum value appears at the edge of mirror surface in the windward, and the wind pressure distribution pattern is similar to that when yaw angle is 45°. When yaw angle is 180°, wind pressure coefficients are all negative, and the maximum value appears at the central part of mirror surface, the wind pressure distribution pattern is similar to that when the yaw angle is 0°.

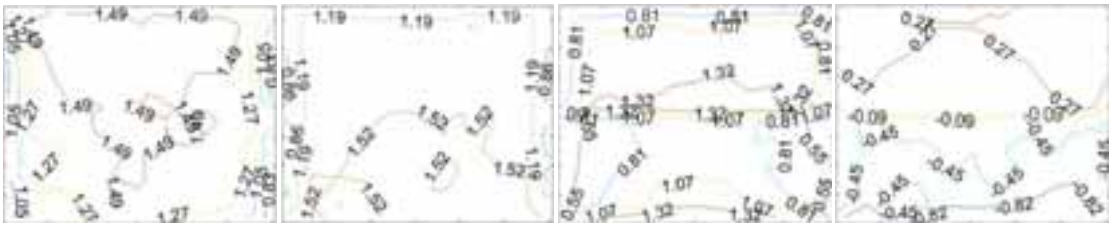

(a) Condition 00-000 (b) Condition 30-000 (c) Condition 60-000 (d) Condition 90-000

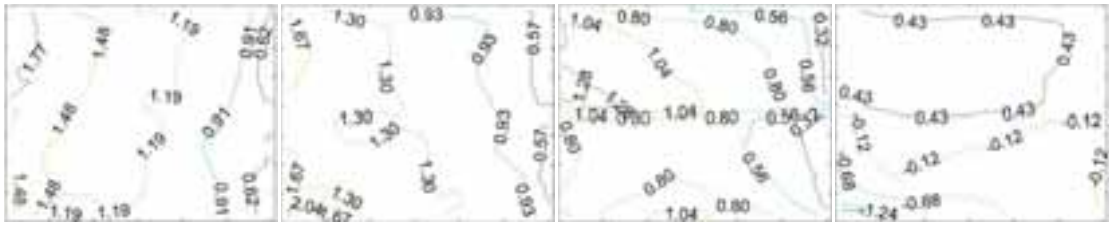

(e) Condition 00-045 (f) Condition 30-045 (g) Condition 60-045 (h) Condition 90-045

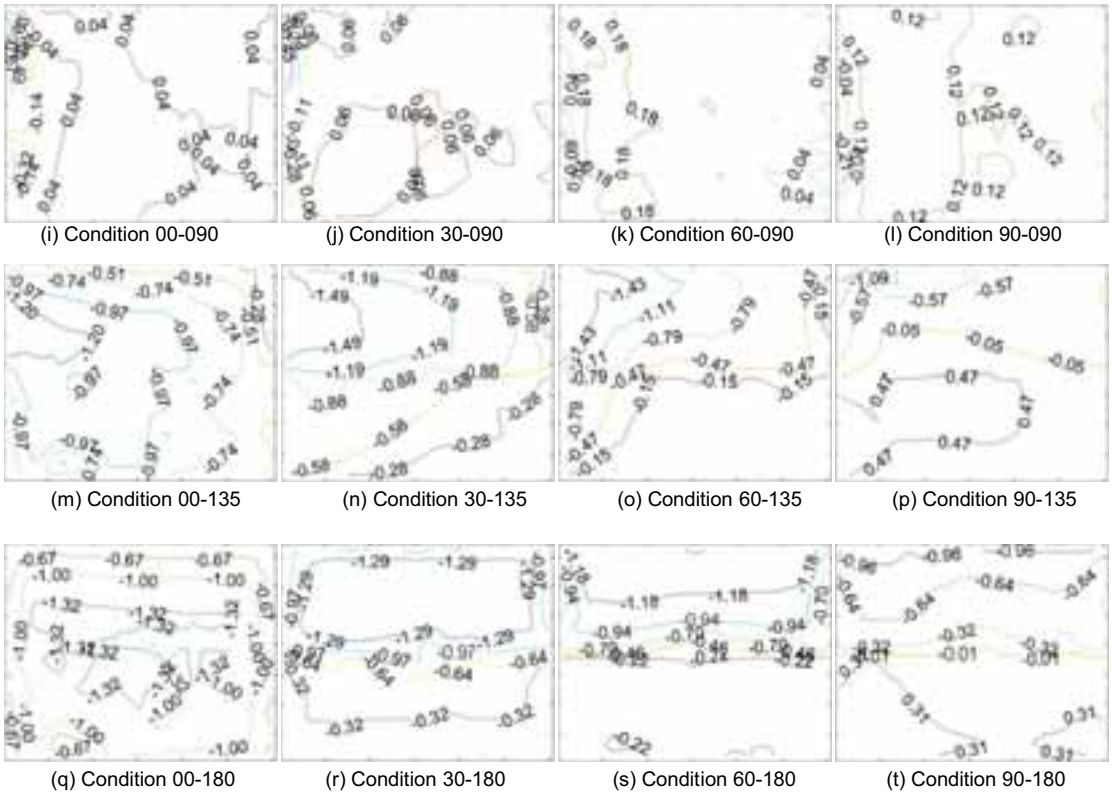

(i) Condition 00-090 (j) Condition 30-090 (k) Condition 60-090 (l) Condition 90-090

(m) Condition 00-135 (n) Condition 30-135 (o) Condition 60-135 (p) Condition 90-135

(q) Condition 00-180 (r) Condition 30-180 (s) Condition 60-180 (t) Condition 90-180

Fig. 8: Contour map of mean wind pressure coefficient at the measuring taps on concentrator surface

4.2. Distribution of fluctuating wind pressure

The contour of fluctuating wind pressure coefficient on mirror surface under typical operating condition is shown in Fig. 9. When yaw angle is 0°, the maximum fluctuating wind pressure coefficient moves toward the edge of mirror surface in the windward as pitch angle increases. This is because cylindrical vortex forms at the edge of mirror surface when air flow reattaches to mirror surface as soon as it is separated by the thin mirror in the windward. Consequently, the maximum fluctuating wind pressure coefficient appears at the edge of mirror surface. When pitch angle increases to 90°, besides the maximum fluctuating wind pressure at the edge of mirror surface, another two maximum wind pressure coefficients appear symmetrically in the central part of mirror surface in leeward. This is resulted from two symmetrical vortices formed in the leeward after the separation of air flow separated at the edge of mirror surface. When yaw angle increases to 45°, fluctuating wind pressure distribution shows a similar pattern despite pitch angle changes. It decreases from the edge of mirror surface in windward to leeward. When yaw angle is 90°, fluctuating wind pressure distribution changes in a gradient pattern because strong air flow separation happens at the edge of mirror surface. When yaw angle is 135°, the fluctuating wind pressure distribution at different pitch angle is similar to the distribution of mean wind pressure. When yaw angle is 180°, the fluctuating wind pressure distributions at pitch angle of 0°, 30° and 60° are similar to the distribution of mean wind pressure. In general, fluctuating wind pressure distribution on mirror surface is similar to the distribution pattern of mean wind pressure.

(a) Condition 00-000 (b) Condition 30-000 (c) Condition 60-000 (d) Condition 90-000

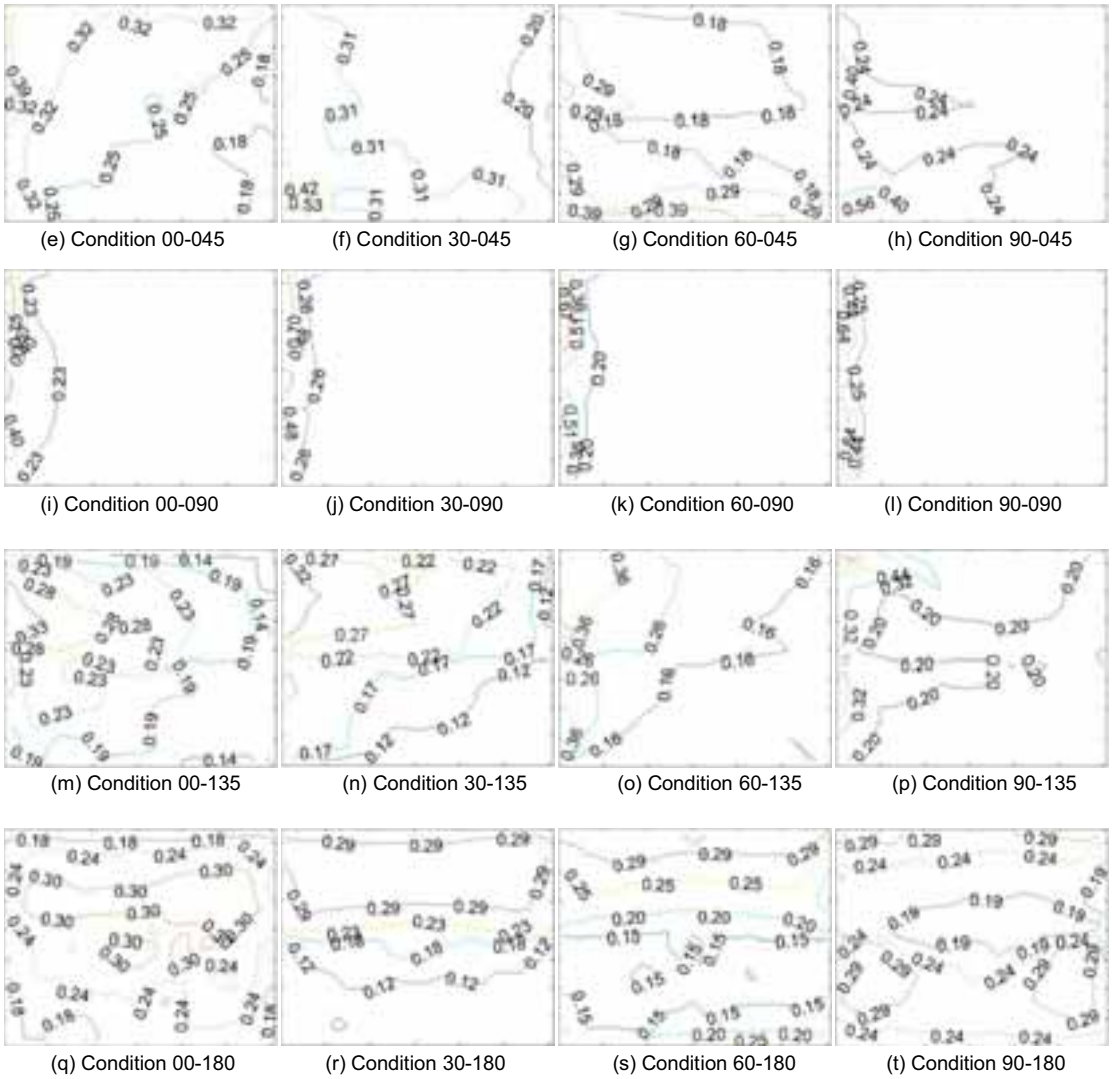

(e) Condition 00-045 (f) Condition 30-045 (g) Condition 60-045 (h) Condition 90-045

(i) Condition 00-090 (j) Condition 30-090 (k) Condition 60-090 (l) Condition 90-090

(m) Condition 00-135 (n) Condition 30-135 (o) Condition 60-135 (p) Condition 90-135

(q) Condition 00-180 (r) Condition 30-180 (s) Condition 60-180 (t) Condition 90-180

Fig. 9: Contour map of fluctuating wind pressure coefficient distribution on concentrator surface

5. Variation of mean wind pressure coefficient with the yaw angles on mirror surface

The variation of mean wind pressure coefficient of some measuring tap on mirror surface with yaw angles are shown in Figure 10. A11, A20 and D6 are measuring taps located near the edge, corner and central part of the same mirror surface (marked as surface A), respectively. The mean wind pressure variation curve of these taps shows the same trend under four pitch angles. When yaw angle is 90^{o}, the mean wind pressure coefficient value changes from positive to negative or vice versa. This is a favorable condition for wind resistance because the wind pressure coefficient value is relatively low. At the pitch angle of 90^{o}, the wind pressure coefficient values of measuring taps A11 and D6 are smaller than that at other three pitch angles. However, a large negative wind pressure coefficient, roughly 2.76, appears at measuring tap A20 at pitch angle of 90^{o} and at yaw angle of 35^{o}. This is quite different from that of heliostat and deserves attention in the process of wind resistant design. T11, T20 and P6 are measuring taps located on the same mirror surface (marked as surface B), and the mean wind pressure coefficient variation curves of these taps are consistent despite the change of pitch angle. With the exception of the measuring tap T20 located at the corner, the solar collector has fortunate condition when the yaw angle and pitch angle are both 90^{o}.

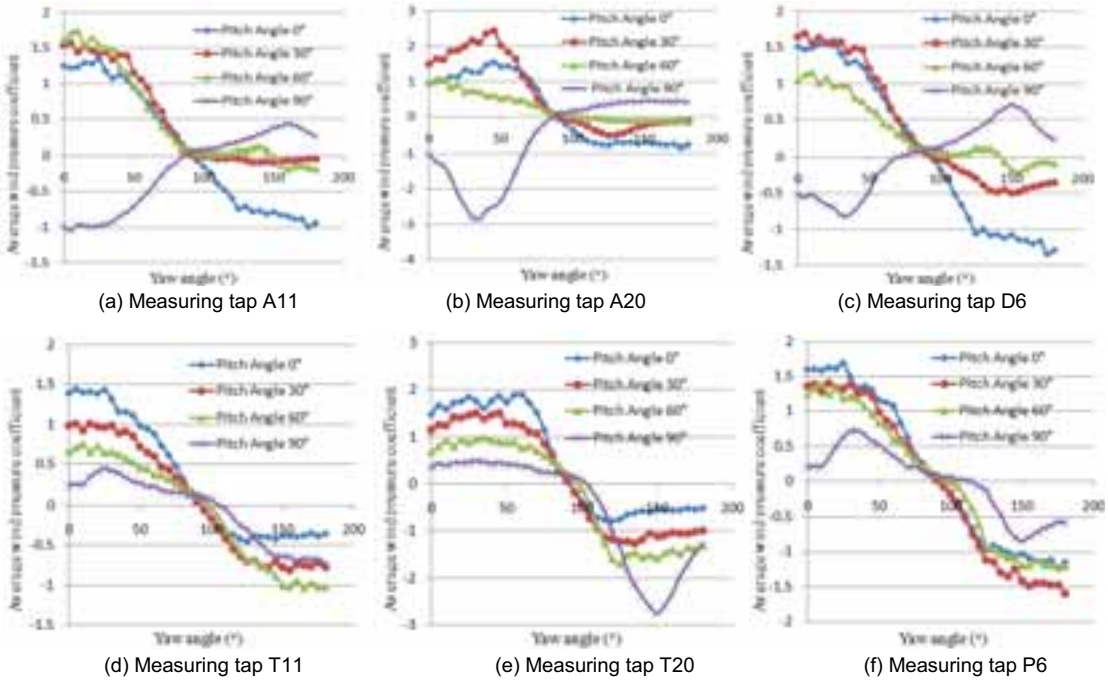

(a) Measuring tap A11 (b) Measuring tap A20 (c) Measuring tap D6

(d) Measuring tap T11 (e) Measuring tap T20 (f) Measuring tap P6

Fig. 10: Mean wind pressure coefficient variation curves at typical measuring taps

6. Extreme wind pressure

Zou Q and Li Z have proved that when pitch angle of mirror surface is large, the wind pressure distribution on mirror surface shows non-Gaussian characteristics. When we calculate the extreme wind pressure coefficients of the non-Gaussian regions on mirror surface by Peak-Factor, the Peak-Factor method is defective for calculating extreme pressure coefficients. Because the peak factor method is based on the assumption that the wind pressure distribution is Gauss distribution. Therefore, in this article we use Hermite moment-based method to calculate the extreme wind pressure coefficients.

Kwon and Kareem (2009) revisit the non-Gaussian peak factor for univariate stationary non-Gaussian processes and clarify the expression of the Hermite moment-based non-Guassian peak factor as (Kareem and Zhao,1994; Kwon and Kareem, 2009):

$$\overline{x}_{ng} = \partial\left\{\left(\beta+\frac{\gamma}{\beta}\right)+h_3\left(\beta^2+2\gamma-1+\frac{1.98}{\beta^2}\right)+h_4\left[\beta^3+3\beta(\gamma-1)+\frac{3}{\beta}\left(\frac{\pi^2}{6}-\gamma+\gamma^2\right)+\frac{5.44}{\beta^3}\right]\right\} \quad \text{(eq. 7)}$$

where γ is Euler's constant (≈ 0.5772); $\beta=\sqrt{2\ln(v_0T)}$; v_0 is the mean zero upcrossing rate of a standardized non-Guassian process $x(t)$, which is obtaind from a general non-Guassian process $X(t)$ as $x(t)=\left[X(t)-\mu_X\right]/\sigma_X$; μ_X is mean value of $X(t)$; σ_X is the standard deviation of $X(t)$; T is time duration; ∂, h_3, h_4 are parameters of moment -based Hermite modle, which gives a transformation from a standard Guassian process $y(t)$ to the standardized ono-Guassian process $x(t)$ as :

$$x(t)=\partial\left\{y+h_3\left(y^2-1\right)+h_4\left(y^3-3y\right)\right\} \quad \text{(eq. 8)}$$

where the parameters h_3, h_4 control the shape of the distribution, ∂ is the scaling factor.

$$\partial=\left(1+2h_3^{\,2}+6h_4^{\,2}\right)^{-\frac{1}{2}},\quad h_4=\frac{\sqrt{1+1.5(\gamma_4-3)}-1}{18}.\quad h_3=\frac{\gamma_3}{4+2\sqrt{1+1.5(\gamma_4-3)}} \quad \text{(eq. 9)}$$

where γ_3 is skewness of a process $x(t)$; γ_4 is kurtosis of a process $x(t)$.

Extreme wind pressure distribution could be derived from equation (7)~(9). Because article length is limited, the maximum and minimum wind pressure coefficient distribution maps on mirror surface under some operating condition are shown in Fig. 11 and Fig. 12, respectively. As shown in the contour, the maximum and minimum values move to the edge of mirror surface with the increase of yaw angle and pitch angle; High pressures are typically concentrated around the edges of the collector because of flow separation or vortex formation from the corner where the most wind damage, such as breakage of the mirror is expected to occur.

(a) Condition 00-000 (b) Condition 30-045 (c) Condition 60-045 (d) Condition 90-050

Fig. 11: The maximum wind pressure coefficient on concentrator surface under typical and the most unfavorable operating conditions

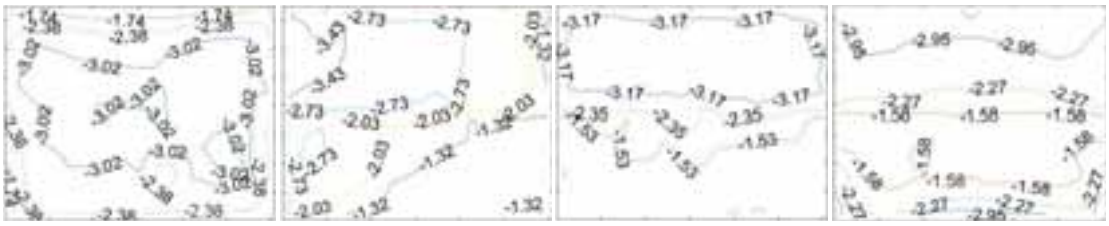

(a) Condition 00-180 (b) Condition 30-135 (c) Condition 30-180 (d) Condition 60-180

Fig. 12: The minimum wind pressure coefficient on concentrator surface under typical and the most unfavorable operating condition

7. Conclusion

- As the pitch angle and the yaw angle increase, wind pressure distribution on mirror surface changes obviously, and the maximum wind pressure coefficient moves toward the edge of mirror surface close to wind.
- High pressures are typically concentrated around the edges of the collector, and the breakage of the reflector panels at the edge is expected to occur. Therefore, the mirror panels should be improved in stiffness of the edge parts to resist wind-induced vibration.
- Peak factor method is not suitable for the calculation of the extreme wind pressure of trough condenser. Because the wind pressure distribution on mirror surface shows non-Gaussian characteristics. In this article , we use Hermite moment-based method to calculate the extreme wind pressure coefficients.
- The wind pressure distribution pattern on mirror surface and wind pressure coefficient value derived from the analysis in the article can be used as reference for the optimization design of concentrator group and the research on mirror surface deformation control.
- Some limiting aspects of the measurement are figured out. Firstly, pitch angle of solar collector could vary from 0^o~360^o. In this study, pitch angles measured are in the range of 0^o~90^o, and these information about wind loads at these pitch angles will be studied in the future. Secondly, this study is research the isolated collector. Actually, in practical engineering solar collectors are work in groups, thus the interference effects of neighboring collector need to be studied in the future.
- All conclusions drawn in the article can be applied to trough concentrator with plane size and height

similar to that of the concentrator in the article. For concentrators whose height and size are quite different from that of the prototype in the article, the wind pressure distribution may deviate from the findings in this article and more research needs to be carried out.

8. Acknowledgments

The work described in this paper was supported by National Natural Science Foundation of China (No:51278190，51178180,51308524).

9. References

Cook, N.J., Mayne, J.R., 1980. A refined working approach to the assessment of wind loads for equivalent static design. J. Journal of Wind Engineering and Industrial Aerodynamics, 6(1): 125-137.

Cook, N.J., Mayne, J.R., 1979. A novel working approach to the assessment of wind loads for equivalent static design. J. Journal of Wind Engineering and Industrial Aerodynamics, 4(2): 149-164.

Gong, B., et al., 2013. Fluctuating wind pressure characteristics of heliostats. J. Renewable Energy, 50: 307-316.

Gong, B., et al., 2012. Field measurements of boundary layer wind characteristics and wind loads of a parabolic trough solar collector. J. Solar Energy, 86, 1880-1898.

Gong, B., et al., 2012. Wind-induced dynamic response of Heliostat. J. Renewable Energy, 38(1): 206-213.

GB50009-2012, 2012. Load Code for the Design of Building Structures, Beijing: China Architecture and Building Press.

Hosoya, N., et al., 2008. Wind tunnel tests of parabolic trough solar collectors. J. National Renewable Energy Laboratory Subcontract Report NREL/SR-550-32282.

Hong, X.J., Gu, M., 2004. The equivalent static pressure and response along-wind. J. Journal of Building Structures, 34(7):39-43.

Kwon D, Kareem A, 2009. Peak factor foe non-Gaussian processes revisited. In Proceeding of the 7th Asia-Pacific Conference on Wind Engineering , Taipei.

Kasperski, M., 2003. Specification of the design wind load based on wind tunnel experiments. J. Journal of Wind Engineering and Industrial Aerodynamics, 91(4): 527-541.

Kumar, K.S., Stathopoulos, T., 2000. Wind loads on low building roofs: a stochastic perspective. J. Journal of structural engineering, 126(8): 944-956.

Kareem A, Zhao J, 1991. Analysis of non-Gaussian surge response of tension leg platforms under wind loads. J. Journal of Off-shore Mechanics and Arctic Engineering, 116:137-144.

Naeeni, N., Yaghoubi, M., 2007. Analysis of wind flow around a parabolic collector (2) heat transfer from receiver tube. J. Renewable Energy, 32(8), 1259-1272.

Pfahl, A., Uhlemann, H., 2011. Wind load on heliostats and photovoltaic trackers at various Reynolds numbers. J. Journal of Wind Engineering and Industrial Aerodynamics. 99(9), 964-968.

Peterka, J.A., Derickson, R.G, 1992. Wind load design methods for ground-based heliostats and parabolic dish collectors. R. Sandia National Labs., Albuquerque, NM (United States).

Peterka, J.A., et al., 1990. Wind loads and local pressure distributions on parabolic dish solar collectors. R. Solar Energy Research Inst., Golden, CO (USA); Colorado State Univ., Fort Collins, CO (USA).

Zou Q, Li Z, Wu H, et al., 2015. Wind pressure distribution on trough concentrator and fluctuating wind pressure characteristics. J. Solar Energy, 120: 464-478.